Band-gap trend of corundum oxides α-M_2O_3 (M = Co, Rh, Ir): An *ab initio* study

Xuefen Cai [1], Su-Huai Wei [2,*], Peter Deák,[2] Cesare Franchini,[3,4] Shu-Shen Li,[1] and Hui-Xiong Deng[1,†]

[1]*State Key Laboratory of Superlattices and Microstructures, Institute of Semiconductors,*
Chinese Academy of Sciences, Beijing 100083, China

[2]*Beijing Computational Science Research Center, Beijing 100094, China*

[3]*Center for Computational Materials Science, Faculty of Physics, University of Vienna, 1090 Vienna, Austria*

[4]*Department of Physics and Astronomy, Alma Mater Studiorum - Università di Bologna, 40127 Bologna, Italy*

In recent years, d^6 transition-metal corundum oxides α-M_2O_3 (M = Co, Rh, Ir) have garnered significant interest due to their notable p-type conductivity; however, their electronic properties remain controversial. In this study, we employ first-principles calculations within different functional levels to systematically investigate the geometry and electronic structure of α-M_2O_3. Our findings reveal that these oxides have a relatively small difference between the indirect and direct band gap, contradicting previous studies. Additionally, we demonstrate that the band gaps of these oxides are closely associated with the ligand field splitting of the cation M d orbitals and the experimentally observed nonmonotonic trend of the direct band-gap variation can be explained by the orbital-dependent Coulomb and exchange interactions. This study enhances our understanding of how the involvement of d orbitals impacts the band gap of transition-metal oxides.

I. INTRODUCTION

Metal oxides typically exhibit n-type conductivity, and achieving p-type doping is a challenge due to the low valence-band energy primarily composed of O $2p$ orbitals. However, recent research has shown that two binary oxides of d^6 transition metals, corundum-type rhodium oxide (α-Rh_2O_3) and iridium oxide (α-Ir_2O_3), exhibit p-type conductivity, making them promising candidates for forming high-quality pn heterojunctions with α-Ga_2O_3 [1–4]. Additionally, the spinel ZnM_2O_4 (M = Co, Rh, Ir) compounds have also demonstrated to be promising p-type oxides and are being studied as transparent conducting semiconductors [5–9]. It is noteworthy that in addition to these remarkable p-type doping properties, α-M_2O_3 compounds also exhibit catalytic properties, rendering them promising for electrocatalysis and photocatalysis [10–12].

Although these d^6 transition-metal oxides (M = Co, Rh, Ir) hold potential promise, until now, their electronic properties, particularly their fundamental band-gap energy, remain poorly understood. Early experimental results for α-Rh_2O_3 (α-Co_2O_3) show both strong and weak absorptions, suggesting a significant difference of $\sim$2.2 eV ($\sim$1.2 eV) between the direct and indirect band-gap values [13,14]. However, the reliability of this interpretation has yet to be confirmed through first-principles calculations. Additionally, given the band-gap observations of Rh_2O_3 and Co_2O_3, it is anticipated that Ir_2O_3 would display a significant direct/indirect gap disparity as well, but recent optical studies suggest only one optical band

gap ($\sim$3.0 eV) for Ir_2O_3 [1,2]. Upon closer examination it becomes apparent that previous experimental studies regarding the band gap of corundum-type Rh_2O_3 and Co_2O_3 were done on powder material with inadequate phase purity. The contaminated samples were likely responsible for the observed low-energy peaks in the experiments for these compounds. Moreover, while spinel ZnM_2O_4 has recently been under intensive research, driven by their p-type transparent conducting properties, the reported band-gap data scatter widely. For instance, the reported optical measurements for $ZnRh_2O_4$ yield a range of 2.0 to 2.7 eV [5,6,15,16]. Therefore, in order to propose useful technological applications for these materials, it is essential to further explore their band-gap energies and electronic properties.

In this work, we focus on studying the electronic properties for the binary M_2O_3 oxides by using first-principles calculations. We have carried out calculations at different levels, using the revised Perdew-Burke-Ernzerhof functional for solids (PBEsol) [17], many-body calculations with the so-called GW method starting from the PBEsol wave function (PBE + G_0W_0) [18], as well as with the Heyd-Scuseria-Ernzerhof functional with mixing parameter α = 0.25 (HSE06) [19], and using also HSE06 + G_0W_0. The results show consistently small direct/indirect gap disparity in all cases, despite a significant variation of the band gaps with the applied method. Based on the specific traits of PBE and HSE functionals, we analyze the association between the localized nature of cation d orbitals, the ligand field splitting, and the band-gap trend for α-M_2O_3 compounds. The insights revealed here not only broaden our understanding of the electronic properties of d^6 transition-metals oxides, but also offer a path to develop better exchange-correlation functionals for accurate modeling of these systems.

*suhuaiwei@csrc.ac.cn
†hxdeng@semi.ac.cn

TABLE I. Calculated lattice parameters a and c of α-M_2O_3 (M = Co, Rh, Ir) using PBEsol functional. Experimental values are listed in brackets. Also shown are fundamental indirect (E_g^{ID}) and Γ-Γ direct (E_g^D) band gaps, as calculated at different levels. Optical band gaps, obtained from HSE06 + G_0W_0 + BSE calculations, and corrected approximately for SOC, are compared to experimentally observed optical band gaps. All band-gap values are given in electron volts (eV).

	Co_2O_3	Rh_2O_3	Ir_2O_3
a (Å)	4.726 (4.782[a])	5.109 (5.108[b])	5.216 (5.23[c])
c (Å)	12.802 (12.96[a])	13.819 (13.81[b])	13.89 (14.01[c])
E_g^{ID} | E_g^D(Calc.)			
PBEsol	0.41 | 0.60	0.60 | 0.88	0.79 | 1.19
HSE06	3.63 | 3.86	2.59 | 2.87	2.62 | 2.95
PBEsol + G_0W_0	1.16 | 1.31	1.48 | 1.77	1.88 | 2.31
HSE06 + G_0W_0	3.87 | 4.03	3.14 | 3.41	3.18 | 3.52
HSE06 + G_0W_0 + BSE + SOC	| 3.4	| 3.2	| 3.1
E_g^O (Expt.)	1.82 | 3.03[d]	1.22 | 3.40[e]	2.93[f]

[a]Reference [22]; [b]Reference [26]; [c]Reference [27]; [d]Reference [14]; [e]Reference [13]; [f]Reference [1].

II. COMPUTATIONAL METHOD

Our study employs calculations based on the projector augmented-wave (PAW) method [20] and density-functional theory (DFT) using VASP (Vienna *Ab initio* Simulation Package) [21]. We utilized the PBEsol functional in the generalized gradient approximation (GGA) [17] for structure optimization, and set the cutoff energy of the plane-wave basis set to 520 eV. The convergence criterion of 1×10^{-3} eV/Å for the Hellmann-Feynman force on each atom was employed, and a Γ-centered $6 \times 6 \times 6$ Monkhorst-Pack (MP) k mesh was used for integration over the Brillouin zone of the 10-atom primitive cell of α-M_2O_3. We have performed spin-polarization tests on α-M_2O_3 (M = Co, Rh, Ir), and found that these oxides exhibit no spin-polarization, falling in line with previous reports [22,23]. As a result, we do not include spin polarization in our calculations. As shown in Table I, the calculated lattice parameters are in good agreement with the experimental data. We compared the performance of different computational methods and functionals for the prediction of band gaps of α-M_2O_3, including PBEsol, PBE + G_0W_0, HSE06, and HSE06 + G_0W_0. Since an accurate G_0W_0 band structure for transition-metal oxides often requires norm-conserving (NC) pseudopotentials [24], we have applied NC-PAWs, developed by the VASP group, for all elements. To ensure convergence of the G_0W_0 calculation, the energy cutoff and the number of energy bands were set to be 800 eV and 800, respectively, while we economized by using a $4 \times 4 \times 4$ MP set. (A test on the HSE06 level showed negligible difference in the band gap, with respect to a calculation with the $6 \times 6 \times 6$ MP set.) We have also performed semi-self-consistent GW_0 calculations [18] on top of HSE06 wave functions for α-Rh_2O_3, and found that the steps beyond G_0W_0 have a negligible effect on the indirect and direct band gap of α-M_2O_3. For a better approximation of the optical band gap, the Bethe-Salpeter equation (BSE) [25] was solved, involving the highest 10 occupied and lowest 10 unoccupied states of the HSE06 + G_0W_0 calculation. The effect of spin-orbit coupling (SOC) on the gap was estimated based on PBEsol and HSE06 calculations.

III. RESULTS AND DISCUSSION

α-M_2O_3 (M = Co, Rh, Ir) adopts a trigonal structure with the space group of $R\bar{3}c$ (No. 167) [Fig. 1(a)]. In this structure, each M cation is at the center of an MO_6 octahedron, surrounded by 6 O atoms, while each O is surrounded by 4 M atoms. As illustrated in Fig. 1(b), the stacking sequence of the cations follows an $ABCABC\ldots$ pattern along the (0001) direction. It should be noted that the cations exhibit a displacement along the (0001) direction towards the vacant octahedral sites, leading to the formation of puckered cation layers and distorted oxygen lattices in the structure. Specifically, the cations are positioned at the $12c$ Wyckoff sites with symmetry of C_3.
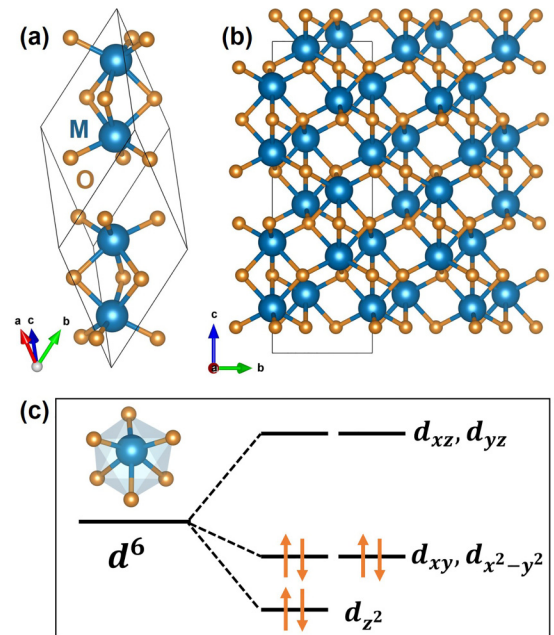

FIG. 1. (a) Primitive and (b) hexagonal cell of corundum α-M_2O_3 (M = Co, Rh, Ir). Dark blue-colored spheres denote cation M, and tawny ones denote O. (c) Energy-level splitting for M d orbitals in distorted octahedral field with C_3 symmetry.

Co, Rh, and Ir are transition metals that occupy consecutive periods in the same group of the periodic table. Co, Rh, and Ir have the $3d$, $4d$, and $5d$ valence electron shells, respectively. As schematically depicted in Fig. 1(c), the distorted MO_6 octahedral ligand field causes the M d^6 state to split into three sets of energy levels. Notably, the d_{xz} and d_{yz} orbitals experience strong interaction with the O atoms along the M–O bonds, making them highest in energy. Conversely, the d_{z^2} orbital has the weakest overlap with the oxygen ligands, and has the lowest energy level. The d_{xy} and $d_{x^2-y^2}$ orbitals exhibit energy levels in between, due to their relatively weaker overlap with the valence orbitals of the O atoms. This order of d-orbital splitting is confirmed by checking the orbital-decomposed electronic structures.

The calculated fundamental indirect (E_g^{ID}) and Γ-Γ direct (E_g^D) band gaps of α-M_2O_3 using different functionals are listed in Table I. The calculated values show significant variation depending on the functional utilized for the calculation. However, the difference between the indirect and direct band gap is invariably small, 0.15–0.23 eV, 0.27–0.29 eV, and 0.33–0.43 eV, depending on the functional, for Co_2O_3, Rh_2O_3, and Ir_2O_3, respectively. While in contrast much larger differences were reported in optical studies of Co_2O_3 and Rh_2O_3, a more recent study on Ir_2O_3 reveals only one optical band gap of 2.93 eV [1]. Earlier optical measurements on Co_2O_3 and Rh_2O_3 show a strong optical absorption at 3.03 and 3.40 eV, respectively, with a much weaker absorption at 1.82 and 1.22 eV, respectively [13,14]. These absorptions are widely attributed to direct and indirect transitions, which would mean a significant difference of 1.21 and 2.18 eV for Co_2O_3 and Rh_2O_3, respectively, between the indirect and direct band-gap values, in stark contradiction to our results at any level of theory.

The measured optical spectra are influenced by excitonic effects, which might be large in these materials (due to the large overlap between electron and hole states) and increasing with the localization of the d states (from Ir to Rh to Co) [28,29]. Therefore, we have performed BSE calculations on top of the HSE06 + G_0W_0 results. To assess the impact of SOC on the band gap of α-M_2O_3 (M = Co, Rh, Ir), we performed comparative calculations using both the PBEsol and HSE06 functionals, with and without SOC. Our findings reveal that SOC has a minimal impact on the indirect and direct band gaps of Co_2O_3 and Rh_2O_3. However, for Ir_2O_3, the inclusion of SOC leads to a slightly larger indirect band gap [0.85 eV (2.66 eV) within PBEsol+SOC (HSE06+SOC)] and a smaller direct band gap [1.12 eV (2.71 eV) within PBEsol+SOC (HSE06+SOC)]. Using the obtained band-gap variation by including the SOC effects, the calculated direct optical gap is shown in the penultimate column in Table I and aligns well with the optical band gap observed in experimental studies.

To better understand the electronic structure of these metal oxides, we present the electronic band structures and partial density of states in Fig. 2, calculated using PBEsol, with a suitable scissors shift Δ applied to the conduction bands to reproduce the experimentally observed direct band gap. All three M_2O_3 compounds exhibit fundamental indirect band gaps, with both the low-dispersion valence- and
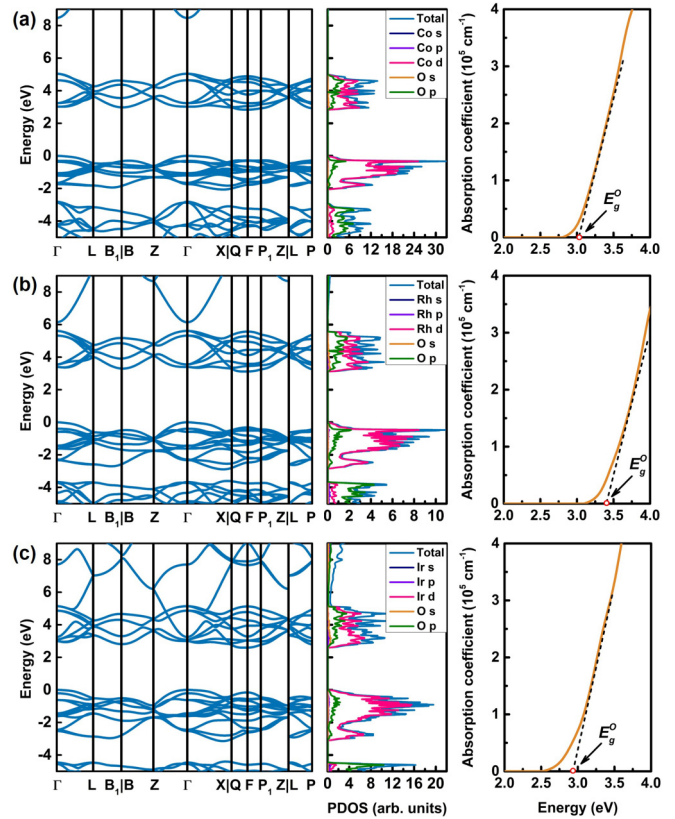

FIG. 2. Electronic band structure, partial density of states, and optical absorption coefficient for (a) Co_2O_3, (b) Rh_2O_3, and (c) Ir_2O_3 calculated using PBEsol + Δ. Valence-band maximum is set at zero.

conduction-band edges being dominated by cation M d orbitals, hybridized with O $2p$ and O $2s$. That is, the band gaps of these oxides basically track the ligand field splitting of M d orbitals. The valence-band maxima are all located at the Γ point, while the conduction-band minima occur along the Q-F direction, a bit lower than the conduction-band edge at the Γ point. With Δ applied in accordance with Table I, the indirect (direct) band gaps for Co_2O_3 are 2.84 (3.03), for Rh_2O_3 are 3.12 (3.40), and for Ir_2O_3 are 2.53 eV (2.93 eV).

One could assume that the notable difference between the two absorptions for both Co_2O_3 and Rh_2O_3, observed in experiments, might be ascribed to dipole-forbidden transitions between the band edges, similar as those observed in In_2O_3 [30] and SnO_2 [31]. To clarify this point, we have also included the calculated optical absorption coefficients in Fig. 2. It is observed that the calculated absorption coefficient shows a sudden increase above the direct band gap. Additionally, the inspection of the wave functions indicates that the valence- and conduction-band edges at the Γ point have the Γ_2^+ and Γ_3^- symmetries, respectively, suggesting the electric-dipole transition between these two states is allowed. Importantly, these observations are consistent across all four functionals used, despite the significantly different band-gap values. Based on these theoretical results, and after close examination of the early optical studies on the band gap of Co_2O_3 and Rh_2O_3 [13,14], we tend to believe that the experimentally observed low-energy peaks can probably be attributed to the low quality

of the powder samples, but not to the indirect transitions of the pure material. The presence of impurities, defects, surface states, and structural disorder in low-quality powder samples can introduce additional energy levels within the material, leading to the observed low-energy peaks. Notably, the 1.82-eV peak in Co_2O_3 closely aligns with the weak band of the yellow *luteo* complex $[Co(NH_3)_6]^{3+}$ [14], whose salts are commonly employed in the preparation of cobalt oxides. This suggests a potential connection between impurities originating from the preparation method and the observed optical features.

In view of the uncertainty in the indirect band gap, we adopt the experimentally observed strong absorption (i.e., the direct band gap) as a benchmark to access the feasibility of different functionals on M_2O_3 compounds. From Table I, it is evident that none of the applied independent-particle methods can closely reproduce the observed band gap of all three oxides. Density-functional theory at the GGA level is known to severely underestimate the band gap of semiconductors due to the inherent self-interaction error [32,33]. It is, therefore, not surprising to observe that PBEsol yields much smaller direct gaps than the experimental values for each M_2O_3. HSE06 bring the results closer to experiment but the scattering is still high. Only the inclusion of many-body effects (*GW* and BSE) improves the situation. It is not common, but sometimes GGA does not even provide an appropriate basis for *GW* calculations and HSE + G_0W_0 is a better option [34]. (We note that self-consistency in *G* is not required in principle, since the screening is already accounted for in HSE06. Indeed, a GW_0 calculation for Rh_2O_3 results in a difference of <0.05 eV with respect to G_0W_0.) The BSE results (with an estimated correction for SOC) for the direct optical gap are closer to the experimental observations. However, in contradiction to those, they give a clear trend among these d^6 transition-metal cations.

To provide a basic physical understanding of the impact of different functionals on the electronic properties of M_2O_3 oxides, we present the calculated Γ-Γ direct band gaps of M_2O_3 as a function of the HSE mixing parameter α in Fig. 3. As expected, the band gap of each oxide increases linearly with the mixing parameter α. However, the slope of Co_2O_3 is considerably bigger than that of Rh_2O_3 and Ir_2O_3, with Rh_2O_3 being slightly bigger than Ir_2O_3. This is consistent with the fact that the Co 3*d* atomic orbitals are more localized, whereas Rh 4*d* and Ir 5*d* atomic orbitals are much more delocalized [35]. For $\alpha = 0$ (i.e., PBE) or for relatively small α values, the band gaps of M_2O_3 are in the order of $Co_2O_3 < Rh_2O_3 < Ir_2O_3$. This can be explained by the fact that the band gap is proportional to the ligand crystal-field splitting and the less-extended 3*d* orbital of Co exhibits weaker *Coulomb interactions* with the ligand orbitals compared to the Rh 4*d* and Ir 5*d* orbitals. However, as α increases, the gradually dominant *exchange potential* pushes down the occupied states and raises the unoccupied states, leading to a larger *d-d* splitting and band gap. This effect is more pronounced with the degree of localization, causing the band gap of Co_2O_3 to increase rapidly. The slightly bigger slope of Rh_2O_3 compared to Ir_2O_3 is because the 4*d* orbital is slightly more localized than the 5*d* orbital. It is observed that beyond a critical value of α (which is ~0.34), the band-gap trend of M_2O_3 reverses, with the order

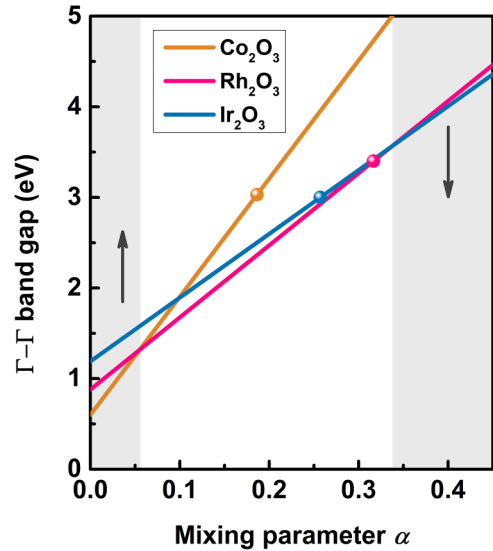FIG. 3. Calculated Γ-Γ direct band gaps of M_2O_3 as a function of HSE mixing parameter α. Upward and downward arrows stand for increasing and decreasing trends of fundamental band gap with increasing cation *M* atomic number (Co → Rh → Ir), respectively. Experimental optical band gaps are indicated by colored spheres.

becoming $Co_2O_3 > Rh_2O_3 > Ir_2O_3$. It is well known that the optimal parameters of HSE are material dependent, due to the simplistic description of electronic screening [36]. As shown in Fig. 3, to obtain accurate band-gap values, different mixing parameters should indeed be employed to account for the different Coulomb and exchange interactions of *M d* orbitals.

IV. CONCLUSION

In conclusion, we have carried out first-principles calculations to study the crystal and electronic structures of α-M_2O_3 (*M* = Co, Rh, Ir) compounds. Contrary to earlier experimental reports, these oxides are consistently found to have a relatively small difference between the indirect and direct band gap, independent of the applied functionals. By analyzing the dependence of the band gap, which is proportional to the ligand field splitting, on the Coulomb and exchange interactions, we have explained the experimentally observed nonmonotonic trend of the band-gap variation from Co_2O_3, Rh_2O_3, and Ir_2O_3. Further experimental confirmations of our predictions and theoretical development of density functional for transition-metal compounds are called for to refine our understanding of the electronic properties of d^6 transition-metal oxides.

[1] J. G. Hao, H. H. Gong, X. H. Chen, Y. Xu, F. F. Ren, S. L. Gu, R. Zhang, Y. D. Zheng, and J. D. Ye, *In situ* heteroepitaxial construction and transport properties of lattice-matched α-Ir_2O_3/α-Ga_2O_3 pn heterojunction, Appl. Phys. Lett. **118**, 261601 (2021).

[2] S.-i. Kan, S. Takemoto, K. Kaneko, I. Takahashi, M. Sugimoto, T. Shinohe, and S. Fujita, Electrical properties of α-Ir_2O_3/α-Ga_2O_3 pn heterojunction diode and band alignment of the heterostructure, Appl. Phys. Lett. **113**, 212104 (2018).

[3] K. Kaneko, S. Fujita, and T. Hitora, A power device material of corundum-structured α-Ga_2O_3 fabricated by MIST EPITAXY® technique, Jpn. J. Appl. Phys. **57**, 02CB18 (2018).

[4] K. Kaneko, Y. Masuda, S.-i. Kan, I. Takahashi, Y. Kato, T. Shinohe, and S. Fujita, Ultra-wide bandgap corundum-structured p-type α-$(Ir, Ga)_2O_3$ alloys for α-Ga_2O_3 electronics, Appl. Phys. Lett. **118**, 102104 (2021).

[5] H. Mizoguchi, M. Hirano, S. Fujitsu, T. Takeuchi, K. Ueda, and H. Hosono, $ZnRh_2O_4$: A p-type semiconducting oxide with a valence band composed of a low spin state of Rh^{3+} in a $4d^6$ configuration, Appl. Phys. Lett. **80**, 1207 (2002).

[6] M. Dekkers, G. Rijnders, and D. H. A. Blank, $ZnIr_2O_4$, a p-type transparent oxide semiconductor in the class of spinel zinc-d^6-transition metal oxide, Appl. Phys. Lett. **90**, 021903 (2007).

[7] T. R. Paudel, A. Zakutayev, S. Lany, M. d'Avezac, and A. Zunger, Doping rules and doping prototypes in A_2BO_4 spinel oxides, Adv. Funct. Mater. **21**, 4493 (2011).

[8] D. M. Ramo and P. D. Bristowe, The effect of defects and disorder on the electronic properties of $ZnIr_2O_4$, J. Chem. Phys. **141**, 084704 (2014).

[9] F.-L. Schein, M. Winter, T. Böntgen, H. von Wenckstern, and M. Grundmann, Highly rectifying p-$ZnCo_2O_4$/n-ZnO heterojunction diodes, Appl. Phys. Lett. **104**, 022104 (2014).

[10] Y. L. Kim, Y. Ha, N.-S. Lee, J. G. Kim, J. M. Baik, C. Lee, K. Yoon, Y. Lee, and M. H. Kim, Hybrid architecture of rhodium oxide nanofibers and ruthenium oxide nanowires for electrocatalysts, J. Alloys Compd. **663**, 574 (2016).

[11] J. Bai, S.-H. Han, R.-L. Peng, J.-H. Zeng, J.-X. Jiang, and Y. Chen, Ultrathin rhodium oxide nanosheet nanoassemblies: Synthesis, morphological stability, and electrocatalytic application, ACS Appl. Mater. Interfaces **9**, 17195 (2017).

[12] C. Diaz, M. L. Valenzuela, O. Cifuentes-Vaca, and M. Segovia, Polymer precursors effect in the macromolecular metal-polymer on the Rh/RhO_2/Rh_2O_3 phase using solvent-less synthesis and its photocatalytic activity, J. Inorg. Organomet. Polym. Mater. **30**, 4702 (2020).

[13] J. Ghose and A. Roy, Optical studies on Rh_2O_3, AIP Conf. Proc. **370**, 901 (1996).

[14] S. P. Tandon and J. P. Gupta, Cobaltic oxide electronic transitions, Solid State Commun. **7**, 1793 (1969).

[15] N. Mansourian-Hadavi, S. Wansom, N. H. Perry, A. R. Nagaraja, T. O. Mason, L.-h. Ye, and A. J. Freeman, Transport and band structure studies of crystalline $ZnRh_2O_4$, Phys. Rev. B **81**, 075112 (2010).

[16] H. Ohta, H. Mizoguchi, M. Hirano, S. Narushima, T. Kamiya, and H. Hosono, Fabrication and characterization of heteroepitaxial pn junction diode composed of wide-gap oxide semiconductors p-$ZnRh_2O_4$/n-ZnO, Appl. Phys. Lett. **82**, 823 (2003).

[17] J. P. Perdew, A. Ruzsinszky, G. I. Csonka, O. A. Vydrov, G. E. Scuseria, L. A. Constantin, X. Zhou, and K. Burke, Restoring the Density-Gradient Expansion for Exchange in Solids and Surfaces, Phys. Rev. Lett. **100**, 136406 (2008).

[18] F. Aryasetiawan and O. Gunnarsson, The GW method, Rep. Prog. Phys. **61**, 237 (1998).

[19] J. Heyd, G. E. Scuseria, and M. Ernzerhof, Hybrid functionals based on a screened Coulomb potential, J. Chem. Phys. **118**, 8207 (2003).

[20] G. Kresse and D. Joubert, From ultrasoft pseudopotentials to the projector augmented-wave method, Phys. Rev. B **59**, 1758 (1999).

[21] G. Kresse and J. Furthmüller, Efficient iterative schemes for ab initio total-energy calculations using a plane-wave basis set, Phys. Rev. B **54**, 11169 (1996).

[22] J. Chenavas, J. C. Joubert, and M. Marezio, Low-spin → high-spin state transition in high pressure cobalt sesquioxide, Solid State Commun. **9**, 1057 (1971).

[23] V. Singh and D. T. Major, Electronic structure and bonding in Co-based single and mixed valence oxides: A quantum chemical perspective, Inorg. Chem. **55**, 3307 (2016).

[24] Z. Ergönenc, B. Kim, P. Liu, G. Kresse, and C. Franchini, Converged G W quasiparticle energies for transition metal oxide perovskites, Phys. Rev. Mater. **2**, 024601 (2018).

[25] M. Rohlfing and S. G. Louie, Electron-hole excitations and optical spectra from first principles, Phys. Rev. B **62**, 4927 (2000).

[26] A. Wold, R. J. Arnott, and W. J. Croft, The reaction of rare earth oxides with a high temperature form of rhodium (III) oxide, Inorg. Chem. **2**, 972 (1963).

[27] W.-H. Chung, D.-S. Tsai, L.-J. Fan, Y.-W. Yang, and Y.-S. Huang, Surface oxides of Ir (111) prepared by gas-phase oxygen atoms, Surf. Sci. **606**, 1965 (2012).

[28] A. L. Allred, Electronegativity values from thermochemical data, J. Inorg. Nucl. Chem. **17**, 215 (1961).

[29] M. Dvorak, S.-H. Wei, and Z. Wu, Origin of the Variation of Exciton Binding Energy in Semiconductors, Phys. Rev. Lett. **110**, 016402 (2013).

[30] A. Walsh, J. L. F. Da Silva, S.-H. Wei, C. Korber, A. Klein, L. F. J. Piper, A. DeMasi, K. E. Smith, G. Panaccione, P. Torelli, D. J. Payne, A. Bourlange, and R. G. Egdell, Nature of the Band Gap of In_2O_3 Revealed by First-Principles Calculations and X-Ray Spectroscopy, Phys. Rev. Lett. **100**, 167402 (2008).

[31] X. Cai, P. Zhang, and S.-H. Wei, Revisit of the band gaps of rutile SnO_2 and TiO_2: A first-principles study, J. Semicond. **40**, 092101 (2019).

[32] A. Zunger, J. P. Perdew, and G. L. Oliver, A self-interaction corrected approach to many-electron systems: Beyond the local spin density approximation, Solid State Commun. **34**, 933 (1980).

[33] J. P. Perdew and A. Zunger, Self-interaction correction to density-functional approximations for many-electron systems, Phys. Rev. B **23**, 5048 (1981).

[34] W. Chen and A. Pasquarello, Band-edge positions in GW: Effects of starting point and self-consistency, Phys. Rev. B **90**, 165133 (2014).

[35] H. Peng, H. J. Xiang, S.-H. Wei, S.-S. Li, J.-B. Xia, and J. Li, Origin and Enhancement of Hole-Induced Ferromagnetism in First-Row d^0 Semiconductors, Phys. Rev. Lett. **102**, 017201 (2009).

[36] P. Deák, M. Lorke, B. Aradi, and T. Frauenheim, Optimized hybrid functionals for defect calculations in semiconductors, J. Appl. Phys. **126**, 130901 (2019).